JOURNAL OF PROPULSION AND POWER
Vol. 16, No. 3, May–June 2000

Streamline Tracing: Technique for Designing Hypersonic Vehicles

Frederick S. Billig*
PYRODYNE, Inc., New Market, Maryland 21774
and
Ajay P. Kothari†
Astrox Corporation, Rockville, Maryland 20850

The methodology for creating a large family of designs of streamline traced planar and axisymmetric inlets for hypersonic airbreathing engines is presented. The subject is introduced by a discussion of streamline tracing of Busemann inlet flowfields, which was the procedure that was used to design the Supersonic Combustion Ramjet Missile (SCRAM) engine. A brief synopsis of test results of SCRAM is presented to demonstrate the efficacy of the streamline tracing technique. The generalized model covers the complete range of flowfields from outward-turning isentropic spikes to inward turning inlets. The radial deviation parameter is introduced as the variable to describe the members of the design family. A variety of inlet shapes and vehicle configurations are shown to demonstrate the design procedure. Arguments are made to support the viability of engine designs based of streamline traces of inward-turning flowfields.

Nomenclature

A	= area
A_i	= inlet area
A_0	= capture area
C	= chord
C_{DADD}	= additive drag coefficients
D_{ADD}	= additive drag
h_0	= height of captured streamtube
r	= radius
r_i	= radius of undisturbed core flow (Fig. 3)
r_0	= radius of the captured and undisturbed core flows
$r_{0\mathrm{ref}}$	= reference radius
r_3	= radius of flowfield following compression
u_r	= radial velocity
u_S	= escape speed
u_θ	= tangential velocity
W_0	= width of captured stream tube
W_3	= width of internal duct
δ^*	= boundary-layer displacement thickness
θ	= flow angle in spherical coordinates or sector angle (Fig. 4)
θ_C	= flow angle in spherical coordinates [Eq. (12), Fig. 8]
θ_d	= flow angle in spherical coordinates [Eq. (13), Fig. 8]
θ_X	= flow angle in spherical coordinates [Eq. (14), Fig. 8]

Subscripts

c, d, x, y, z	= points in internal flowfields
f, g, h	= points in freestream flowfield
ref	= reference value
3	= internal duct

Presented as Paper 97-7197 at the AIAA-ISABE XIII International Symposium on Air Breathing Engines, Chattanooga, TN, 8–12 September 1997; received 11 May 1998; revision received 23 April 1999; accepted for publication 26 April 1999.

*President, 11280 Panorama Drive; PYRODYNE@aol.com. Fellow AIAA.
†President, 1350 Piccard Street, Suite 320. Member AIAA.

Introduction

THE conceptual design of a configuration is the fundamental first step in the development of a vehicle for an airbreathing hypersonic application. Typically, it is the product of an innovative individual or design team and is based on the extension of previously examined configurations. Moreover, it usually represents a very limited class of engine flowpaths and, even with modifications, still only covers a small area of the potential design space. This paper introduces a generalized design methodology that both significantly broadens the coverage of the design space and provides the guidance required to select an optimal engine design, subject to imposed constraints.

The foundation upon which this design and evaluation tool is built is a computer-based method that generates streamline traces through axisymmetric and planar flowfields. Long before the advent of high-speed computers, streamline tracing was successfully, albeit laboriously, used to design the Supersonic Combustion Ramjet Missile[1] (SCRAM). Although nearly 30 years have passed, the performance demonstrated in the ground tests of the SCRAM engine remains the benchmark in liquid-fueled scramjets. It is instructive to introduce the contemporary, more generalized method of streamline tracing with a terse description of the procedures that were used to design the SCRAM engine.

Busemann-Inlet Design Methodology

The full Busemann-inlet flowfield, from which streamline surfaces are cut, is a conical, inward-turning, axisymmetric flowfield that terminates in a conical shockwave.[2] Figure 1 is a schematic illustration of the flowfield. At the design point Mach number Mach waves emanating from the curved inward-turning surface coalesce at the apex, O of the internal conical shock. The conical isentropic compression, in which flow conditions along a ray from the origin are constant, is described mathematically in terms of u_r and u_θ, which represent the radial and tangential velocity components in a spherical coordinate system, nondimensionalized with respect to the escape speed u_S. The governing relationship is the Taylor–Maccoll equation for axisymmetric conical flow:

$$\left(u_r'^2\right)(u_r + u_r'') = [(\lambda - 1)/2]\left(1 - u_r - u_r'^2\right) \cdot \left(u_r'^2 - u_r' \cot\theta + 2u_r\right) \tag{1}$$

The velocity component u_θ is related to u_r by the irrotationality condition:

$$u_\theta = u_r' = \frac{\mathrm{d}u_r}{\mathrm{d}\theta} \tag{2}$$

At the design Mach number the conical internal shock turns all of the flow coaxially, and inviscid losses are remarkably small. With the properties defined on the outermost streamline of the inviscid flowfield, a momentum integral technique was used to calculate the displacement thickness and in turn, the adjusted surface geometry. At other than the design Mach number, coalescence of the Mach waves at a point is not realized, and the terminal shock is not conical. Additional uncancelled compression and expansion waves are present, and the corresponding efficiencies are lower than would be obtained in an on-design inlet. Nonetheless, the overall compression efficiency of these inlets is high relative to other types of compression fields. The fundamental problem is that the inlet will not start in steady flow. To circumvent this problem, the compression field can be cut into sectors along streamline surfaces and then reassembled into a viable shape suitable for a vehicle inlet. This is one example of the streamline-tracing technique.

Whereas, at the design Mach number, the inviscid Busemann flowfield calculations for the SCRAM inlets produce shock-free flow upstream of the internal conical shock, the resulting inlet surfaces have razor thin leading edges. The δ^* correction slightly exacerbates this problem. Noting that the inlet is only a point design, i.e., at a single Mach-Reynolds-number condition, a design compromise was adopted. The leading-edge surfaces were shortened and slightly blunted, and the initial compression surface was changed to a small-angle internal cone that is blended into the isentropic surface. A weak shock is formed on the leading edge, and the flow downstream contains a small entropy gradient. The associated total pressure loss is trivial, and the impact of the entropy gradient on the downstream wave structure is minimal.

Figure 2 depicts the strategy used in the design of the SCRAM engine of segmenting the flow into discrete modules. In the upstream plane the streamlines that are followed originate along the straight lines A-B and B-C, and the circular arc B-O-C as shown in the front view. At the end of compression, the streamlines pass through X-Y-O-Z-X. The contoured inlet leading edges illustrated in the angular view are obtained by projecting lines AB, AC, and B-O-C onto the leading-edge Mach cone of the full inlet. Ahead of the intersection with the Mach cone, the surfaces are cut out; thus, the open area B-O-C provides a zone for supersonic spillover when the inlet is operated below its design Mach number. The body of the inlet is then cut longitudinally along AB and AC and reassembled to form a modular inlet that is cylindrical on the periphery. As shown, the angle B-A-C is 90 deg, and the resulting reconstructed vehicle has four independent flowpaths. In the final design of SCRAM, the angle B-A-C was increased to 120 deg to form three independent flowpaths. Both three- and four-module designs were tested in the SCRAM inlet development program.

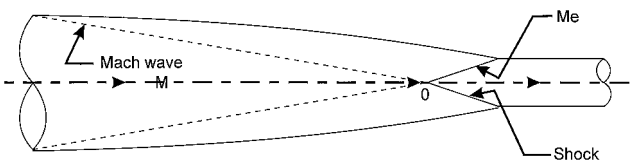

Fig. 1 Busemann inlet.

Generalized Streamline-Tracing Method

This method also begins with the calculation of inviscid inlet flowfields, which, as in the SCRAM design, are subsequently modified to account for the displacement thickness, before defining the surface geometries. An entire family of inlet flowfields varying from outward turning axisymmetric, generated by an isentropic spike as typified by the inlet of the SR-71, to a fully internally turning, similar to the Busemann type, can be examined. The formulation of the solution of the flowfields is the introduction of the radial deviation parameter (RDP)[3] for axisymmetric flows. This parameter, which ranges in value from negative one to positive one, spans a continuous spectrum from maximum outward turning (RDP = −1.0) to two-dimensional planar (RDP = 0.0), to maximum inward turning (RDP = +1.0).

Radial deviation parameter:

$$\mathrm{RDP} = \Delta r / r_0 \tag{3}$$

Inward turning:

$$\mathrm{RDP} = \frac{r_0 - r_i}{r_0} \tag{4}$$

Outward turning:

$$\mathrm{RDP} = \frac{r_i - r_0}{r_0} \tag{5}$$

The effect of radial deviation for the inlet flowfield is incorporated into the classical axisymmetric method-of-characteristics solution with the introduction of core flow. Core flow, as shown in Figs. 3a and 3b, is simply a uniform undisturbed stream tube with a uniform cross section. It is centered on the streamwise axis of the axisymmetric solution. The method of characteristic mesh then surrounds the core. In principle, the core can either be undisturbed freestream flow or a solid body. As in the case of the Busemann inlets, the characteristics

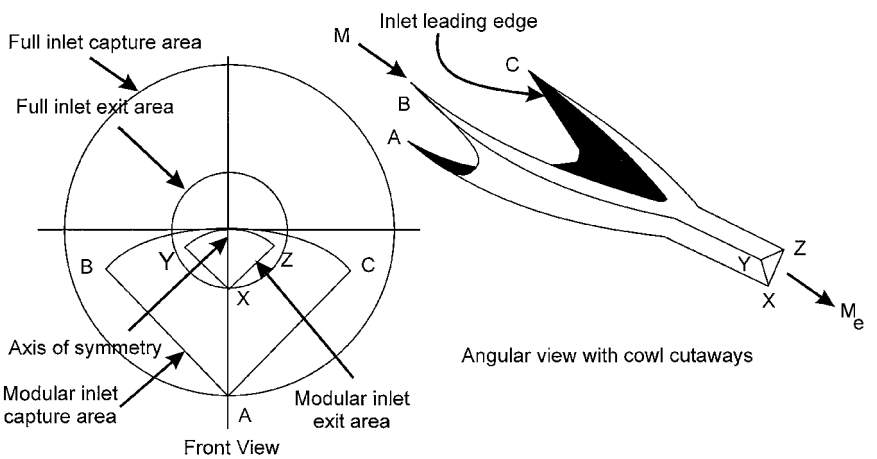

Fig. 2 Streamline-tracing technique for design of modular Busemann inlet.

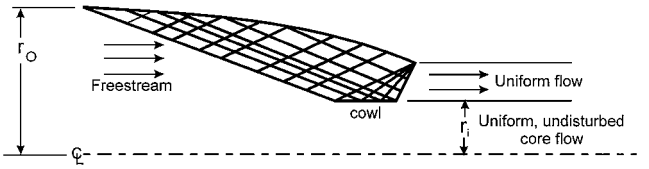

a) Inward turning

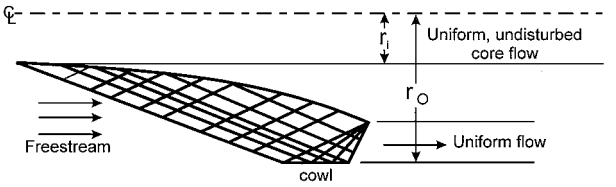

b) Outward turning

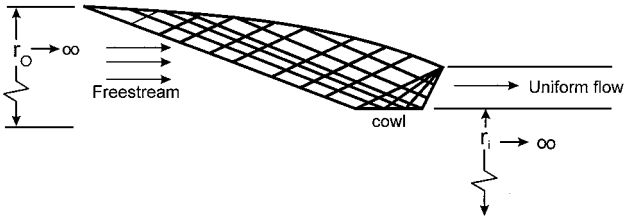

c) Planar

Fig. 3 Core flow as introduced in the definition of the radial deviation parameter.

that initiate the compression can be replaced by a weak conical shock, and the razor sharp leading edges can be slightly blunted in practical designs.

From the axisymmetric flowfield solution a cross section of a desired shape can be selected in either the freestream or at the end of the compression field. The corresponding streamlines are then traced, either upstream or downstream to define the inviscid inlet surfaces. With flow properties defined on the inviscid surfaces, the boundary layer is calculated, and the surface geometry is adjusted by δ^*.

With the flow properties at the end of the inlet defined, the combustor-inlet isolator is designed using the correlation given in Ref. 4, or another suitable alternative procedure. A variety of methods, spanning quasi-one-dimensional to finite difference with complex kinetics, are used to compute the combustor flow. The nozzle flowfield is generated using the method of characteristics similar to that used in the design of the inlet geometries. The external covering geometry is then defined to join the inlet capture and nozzle exit areas and to produce a specified external shock strength along the leading edge. Wings are then sized to meet some design criteria, such as lift at takeoff, and are added to the configuration.

A fundamental design parameter for airbreathing engines is the inlet contraction ratio (CR), i.e., cross-section area of the freestream air captured in the inlet/cross-sectional area of the flow following compression. For axisymmetric inlets, or sectors thereof

Axisymmetric inlet, Compression ratio,

Inward turning:

$$\mathrm{CR}_A = \frac{r_0^2 - r_i^2}{r_3^2 - r_i^2} \tag{6}$$

Inward turning:

$$\mathrm{CR}_A = \frac{r_0^2 - r_i^2}{r_0^2 - r_3^2} \tag{7}$$

where r_3 is the radius of the flowfield following inlet compression.

As a first example of the use of streamline tracing for preliminary design, consider the case of a family of axisymmetric sector

Table 1 Geometry of inlets shown in Fig. 3b

			$\mathrm{CR}_A = 6$			
RDP	r_i/r_0	r_i/r_0	θ, deg	$r_0/r_{0\,\mathrm{ref}}$	$r_i/r_{0\,\mathrm{ref}}$	$r_3/r_{0\,\mathrm{ref}}$
1.00	0.00	0.4082	110.00	1.0000	0.0000	0.4082
0.67	0.33	0.5074	95.66	1.1360	0.3749	0.5764
0.34	0.66	0.7278	51.05	1.9539	1.2896	1.4220
0.00	1.00	——	——	——	——	——
−0.34	0.66	0.9518	51.05	1.9539	1.2896	1.8597
−0.67	0.33	0.9228	95.66	1.1360	0.3749	1.0483
−1.00	0.00	0.9129	110.00	1.0000	0.0000	0.9129

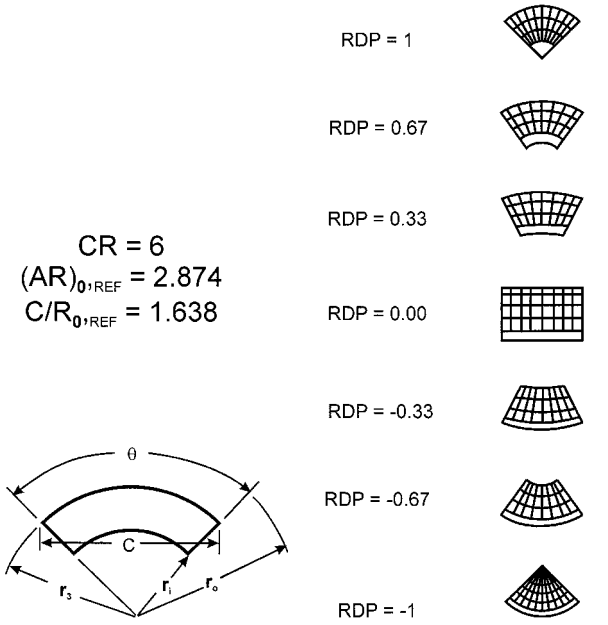

a) Nomenclature **b) Frontal views of inlets**

Fig. 4 Effect of radial deviation parameter on inlet shapes.

inlets with RDP varying from +1 to −1, constrained to have the same CR_A, equal air capture A_0, and chord C. Figure 4a shows the Nomenclature used in describing these geometries. The exercise begins with the simultaneous solution of

$$c/r_0 = 2\sin(\theta/2) \tag{8}$$

and

$$A_0/r_0^2 = \pi\left[1 - \left(r_i^2/r_0^2\right)\right](\theta/360) \tag{9}$$

with $r_i = 0$ to determine the limiting values of the design parameters. Because θ can vary from 0 to 180 deg, the maximum $A_0/r_0^2 = 1.5708$ and the maximum $c/r_0 = 2$ at $\theta = 180$ deg, where $c/h_0 = 2.565$ for the corresponding inlet having an equal A_0. Of interest is the RDP = 0 inlet that has the maximum c/h_0. This occurs at $\theta = 133.6$ deg with $c/h_0 = 2.989$.

The next step is to select a value of θ for RDP = 1, which establishes $(c/h_0)_{\mathrm{Ref}}$ where $r_{0\,\mathrm{ref}}$ is the value of r_0 for RDP = 1. In this example $\theta = 110$ deg at RDP = 1 was chosen, which yields $(A/r_0)_{\mathrm{Ref}} = 0.95943$, $(c/r_0)_{\mathrm{Ref}} = 1.6838$, $(h/r_0)_{\mathrm{Ref}} = 0.5859$, $(c/h_0)_{\mathrm{RDP}=0} = 2.796$. Values of θ for other RDP can then be found from the simultaneous solution of Eq. (8) and (9). The CR_A then establishes the values of r_3 from Eq. (6) and (7). In this example the values for CR_A is 6. Table 1 and Fig. 4b show the results for this family of inlets. Having established a set of inlets subject to selected design constraints, a family of vehicles can be designed to establish the sensitivity of vehicle design parameters to variations in RDP.

HAVDAC,[3] a versatile interactive computer code, can be used to generate the geometry of both the internal and external surfaces.

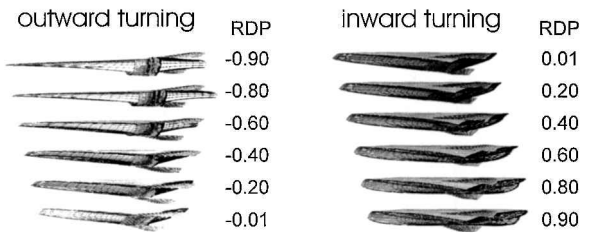

Fig. 5 Vehicles designed using sectors of axisymmetric flowfields with various RDP.

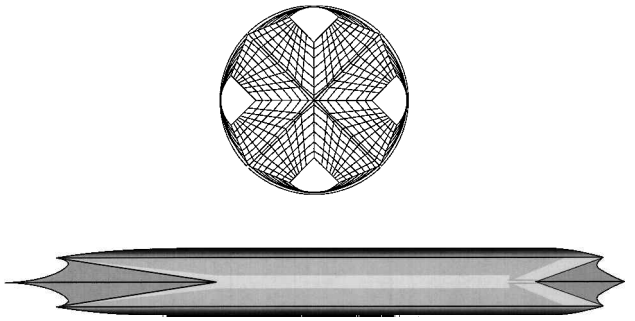

Fig. 6 Front and top views of four-module vehicle formed from sectors of RDP = 1.

Figure 5 from Ref. 3 shows typical displays that are generated. As expected, this more generalized streamline tracing method upon which HAVDAC was developed can also produce similar geometries to those of the Busemann family when RDP is set to one. Figure 6 shows such a four-module vehicle with a crown inlet constructed from four $\theta = 90$-deg sectors.

The preceding examples are sectors of axisymmetric or planar flows, wherein the lateral surfaces are radial slices through the flowfields. In multimodular configurations the modules were joined along these flat radially sliced surfaces. The streamlines that are traced all lie in the flat surfaces. When other than radial slices are made, the surfaces have compound curvature, and tracing the streamline is more complex. To address this complexity, consider a design requirement to produce an internal duct geometry that has a rectangular cross section. Additionally, both the aspect ratios of the inlet capture area, $AR_0 = W_0/h_0$ width/height and of the internal duct $AR_3 = W_3/h_3$, are design constraints. A key feature of this engine design could be moveable hinged sidewalls in the internal duct. By moving these walls inboard, the overall contraction ratio of the engine could be varied.

For planar configurations RDP = 0; the solution is simple, but the results may be unsatisfactory. The value of the aspect ratio AR_3 is simply $AR_0 \times CR$. Because CR for the hypersonic vehicle ranges from 4 to 40, the resulting configurations have large AR_3, which leads to large internal surface areas with high cooling requirements and relative high friction. For large vehicles the shallow height of the combustors can be advantageous because of the simplification of the fuel injection and distribution, but for small vehicles this generally is not an important consideration.

For RDP = 1 designs the cross section of the flowfield at the end of the inlet compression is geometrically similar to the cross section of the capture flow in the freestream. For a rectangular internal duct the respective dimensions are proportional to the square root of the CR, e.g., $h_3 = CR^{1/2} \times h_0$ and $AR_3 = AR_0$. These RDP = 1 vehicles are the most interesting configurations for many applications. Their intrinsic attributes will be discussed later. Whereas the entrance and exit cross sections are rectangular in the RDP = 1 inlet, at all intermediate planes the cross-sectional contours are complex shapes. Figure 7 shows the evolution of these contours for the particular case of a high contraction inlet (CR = 25) with $(AR)_3 = (AR)_0 = 2$. Nozzle expansions will have similar characteristics. Nontheless, there are several test facility nozzles that are in use, which have attempted to generate rectangular cross sections with lateral expansion on the

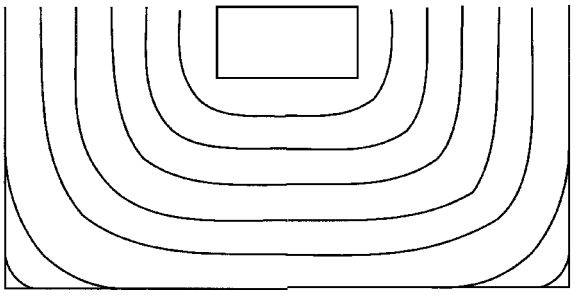

Fig. 7 Cross-section contours of high contraction (CR = 25) RDP = 1 with rectangular through duct.

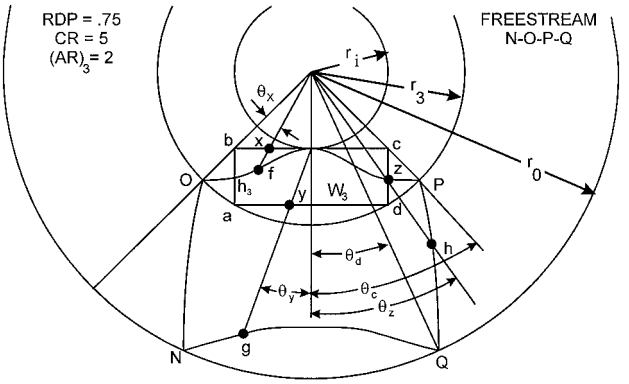

Fig. 8 Generation of cross-sectional area in freestream from rectangular flowfield of internal duct.

orthogonal walls. As would be expected, the resulting flowfields are highly distorted.

The geometry for a $0 < RDP < 1$ inlet is generated by tracing streamlines upstream from the rectangular through duct. Figure 8 shows the cross-sectional areas of the internal duct with $(AR)_3 = 2$ and the corresponding cross-sectional area in the freestream for CR = 5 and RDP = 0.75. It also shows the nomenclature for generalized solutions of the surfaces for RDP $\neq 0$ or 1.

The line b-c is tangent to the uniform core flow at the vertical axis of the flowfield. A selected AR_3 sets the lengths of b-c $= W_3$, b-a and c-d $= h_3$, where a and d lie on the arc having a radius $= r_3$. The equations for r_3/r_0 and W_3/r_0 in terms of CR, RDP, and $(AR)_3$ are

$$r_3/r_0 = \{1/CR + (1 - RDP)^2[1 - (1/CR)]\}^{\frac{1}{2}} \tag{10}$$

$$\frac{W_3}{r_0} = -\frac{2(1 - RDP)}{(AR)_3} + \left\{\frac{4(1 - RDP)^2}{(AR)_3^2} + \left[\frac{4}{(AR)_3^2} + 1\right]\left[\frac{r_3^2}{r_0^2} - (1 - RDP)^2\right]\right\}^{\frac{1}{2}} \Bigg/ \frac{2}{(AR)_3^2} + \frac{1}{2} \tag{11}$$

θ_d and θ_c are the angles between the vertical axis and radius that pass through points d and c, respectively.

$$\theta_d = \sin^{-1}[W_3/2r_3] \tag{12}$$

$$\theta_c = \tan^{-1}[W_3/2r_i] \tag{13}$$

The streamline passing through point X on line b-c, where

$$r_i/r_x = \cos\theta_x \tag{14}$$

is generated from point f in the freestream where

$$r_f/r_i = \left\{1 + CR\left[\left(r_x^2/r_i^2\right) - 1\right]\right\}^{\frac{1}{2}} \tag{15}$$

The streamline passing through point Y on line a-d, where

$$\frac{r_i + h_3}{r_y} = \cos\theta_y \tag{16}$$

is generated from point g in the freestream where

$$r_g/r_i = \left\{1 + \mathrm{CR}\left[\left(r_y^2/r_i^2\right) - 1\right]\right\}^{\frac{1}{2}} \tag{17}$$

The streamline passing through point Z on line c-d, where

$$W_3/2r_z = \sin\theta_z \tag{18}$$

is generated from point h in the freestream where

$$r_h/r_i = \left\{1 + \mathrm{CR}\left[\left(r_z^2/r_i^2\right) - 1\right]\right\}^{\frac{1}{2}} \tag{19}$$

SCRAM Test Results

Figure 9 shows photographs of the inlet test models, and Table 1 summarizes the test results of the SCRAM inlet. These inlets had a design Mach number of 7.8 and were self-starting at Mach number below 4. The air-capture characteristics and compression efficiencies of these fixed geometry inlets are competitive with, if not superior to, planar and outward-turning (e.g., isentropic spike) inlets. Stable inlet operation at up to 12-deg angle of attack in the leeward orientation and up to 15-deg angle of attack in the windward orientation was remarkable. Figure 10 shows Mach-number profiles in the three module SCRAM inlet when tested at 0-deg angle of attack. Data are shown for test Mach numbers of 5.29 and 4.00. Both the radial and circumferential Mach number distortion have only small distortion, considering that the inlet is operating below the design Mach number. These characteristics established the Busemann class of inlets as ideal candidates for maneuvering missile applications.

Whereas the cross-sectional shape of the flow field at the exit of a segmented Busemann inlet is semi-elliptical, the direct-connect combustor tests were carried out in geometries with circular cross sections. It was hoped that an injector/combustor design that yielded high combustor efficiency in the direct-connect test would only have to be slightly modified and would produce similar high efficiency in the free-jet engine tests. This turned out to be the case.

References 5 and 6 discuss the methodology that was used to design the exhaust the nozzle of SCRAM. A method of characteristics

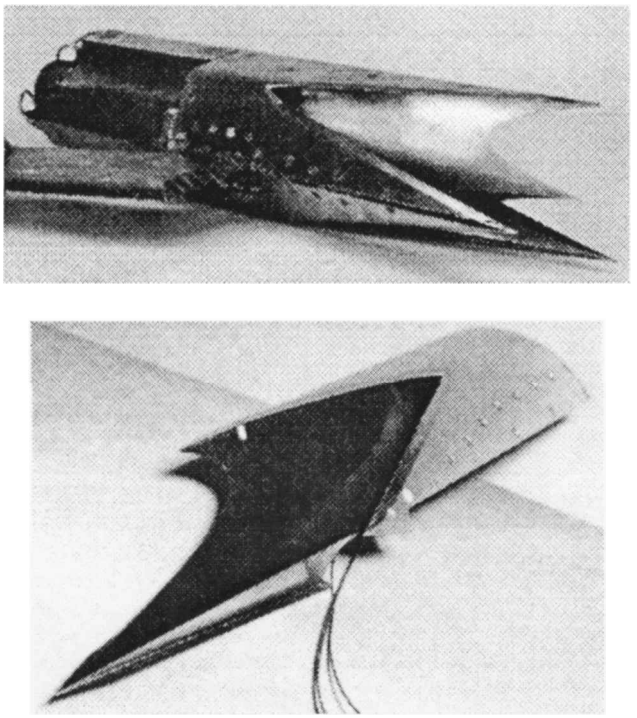

Fig. 9 Photographs of inlet test models.

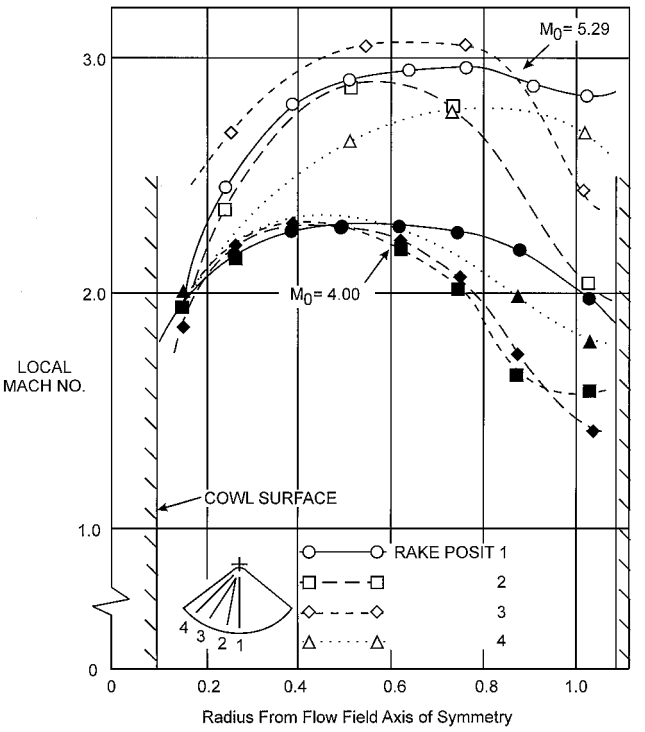

Fig. 10 SCRAM three-module inlet investigation Mach profiles at station 16.5, α = 0 deg.

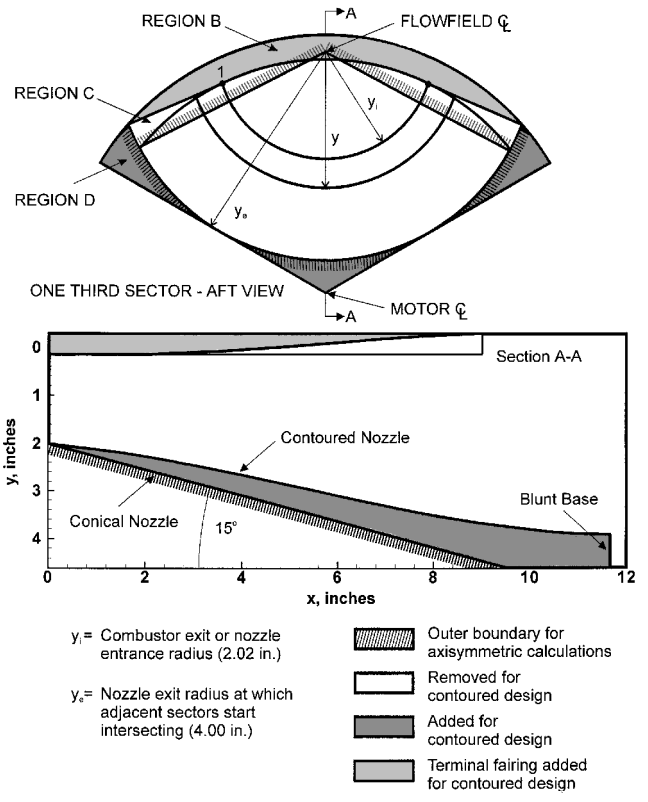

Fig. 11 SCRAM engine test model exhaust nozzle.

with chemical reactions computer program was developed to calculate numerous axisymmetric nozzle expansions. Flow properties in the entrance plane were taken as uniform. The initial conditions were obtained from cycle calculations for the entire range of flight Mach numbers and engine-operating equivalence ratios (ER). Streamline surfaces were cut from the calculated flowfields in a similar method to that used in the inlet design. These surfaces were superposed, and a compromise reference surface was adopted as shown in Fig. 11.

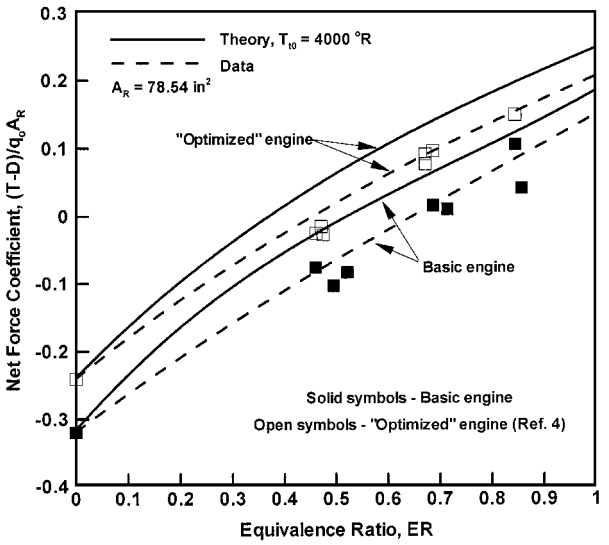

Fig. 12 Net force coefficients for hypersonic engine HiCal 3-D fuel, M_0 = 6.91 − 7.02.

Another 15-deg half-angle conical shape nozzle was used in the initial tests of the SCRAM engine at Mach numbers of 5 and 5.8 because the contoured nozzle design technique had not yet been developed at the time. The improved performance materialized when the contoured nozzle was installed in SCRAM and tested at Mach 7.2 at John Hopkins University, Applied Physics Laboratory.[7]

Net force coefficients for tests with HiCal-3D fuel at Mach numbers of 6.91–7.02 are shown in Fig. 12. The theoretical curves are based on measured inlet efficiencies, calculated nozzle efficiencies, a specified combustion efficiency, calculated internal shear and heat losses, and external drags from aerodynamic wind-tunnel tests.[8] Additive drag coefficients $C_{\mathrm{DADD}} = D_{\mathrm{ADD}}/q_o A_R$ from the inlet tests are 0.0521 at $T_{\mathrm{to}} = 4000$°R based on a reference area $A_R = 78.54$ in^2. External drags include a cowl-lip drag coefficient of 0.011, friction drag of 0.035 for the short isolator-step geometry, and a base drag coefficient for the basic engine, which varies from 0.002 at ER = 0 to −0.004 at $\mathrm{ER}_{\mathrm{eff}} = 1$. The correction for heat loss is quite significant varying from an ER change of 0.05 at ER = 0–0.19 at ER = 1. The agreement between the measured and calculated net force coefficients at ER = 0 gives credence to the approach for estimating efficiencies and losses. The data points with combustion correspond to combustion efficiencies of 0.80–0.85. The expected increase in performance with the contoured exit nozzle in the optimized engine was observed and highlights the importance of nozzle design if maximum efficiency is to be realized in scramjet engines. The demonstration of thrust equal to drag at an ER = 0.5 in the optimized engine clearly established the viability of the scramjet as an effective accelerator to flight speeds greater than Mach 7.

Application of HAVDAC

Conceptual designs for four different vehicle configurations are shown in Fig. 13. Figure 13a is a planar design (RDP = 0) that is similar to National Aerospace Plane (NASP) configuration and serves as a reference to evaluate distinctly different concepts as exemplified by Figs. 13b, 13c, and 13d. All three of these have inward-turning inlet compression fields and the reverse process in the nozzle traced from RDP = 1 axisymmetric flowfields. Applications for these designs include horizontally or vertically launched vehicle for transatmospheric accelerators, hypersonic cruise aircraft, and expendable missiles. All have swept leading edges that minimize heat transfer and drag and provide for spillage to enhance starting. If needed, relatively simple techniques can be used to relieve the internal contraction of the inlet for low-speed operation. A short section of the cowl crotch surface can either be translated aft or rotated circumferentially. As in the SCRAM inlet, the flow into the combustor is more uniform over a wider range of flight speeds than for planar designs. The configuration shown in Fig. 13b has

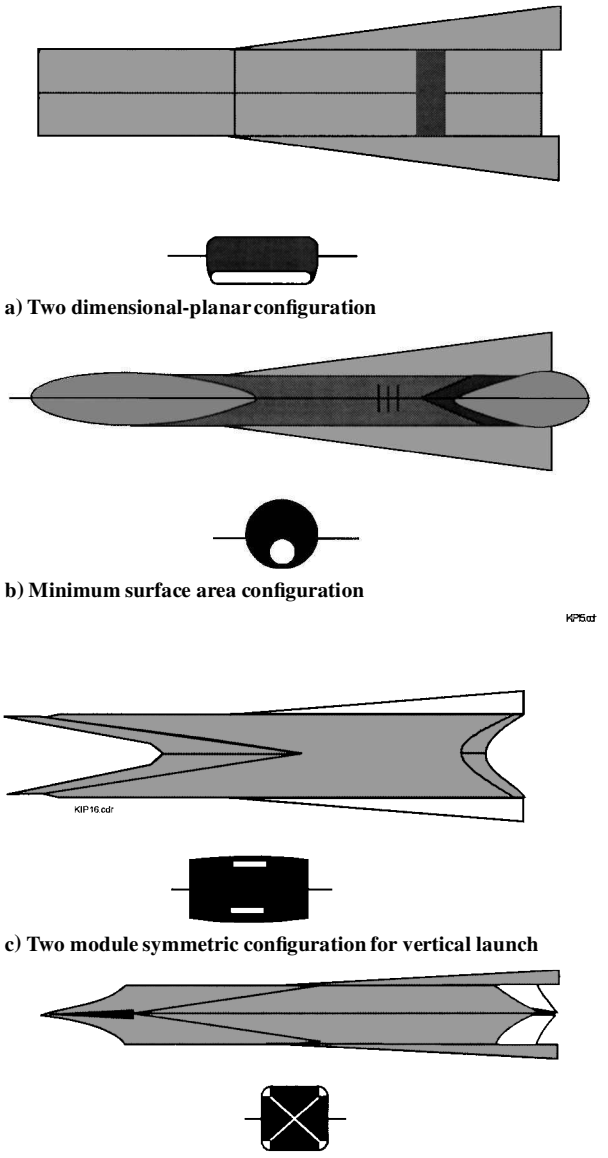

Fig. 13 Conceptual design of four different single-stage space access vehicles.

an inlet surface that is a circular cut tangent to the axis of symmetry of the basic flowfield. The resulting internal ducts have circular cross sections, which leads to a number of beneficial features. For a given flow area the surface area is minimum, thereby minimizing the shear and heat transfer. Thermal and pressure stresses are also minimized. These combined attributes lead to a large reduction in structural weight and considerably lower cooling requirements. Figures 13c and 13d are symmetric about one and two axes, respectively. For these designs the resultant thrust vector is aligned with the vehicle axis, which leads to a large reduction in the trim requirements. As the number of modules increases, the wetted surface area also increases, but the length of the inlet and nozzle decrease. Studies currently underway are to assess which of the configurations are optimal for the different applications.

Conclusions

Streamline tracing of exact solutions of two-dimensional flowfields, planar or axisymmetric, provide the designer with a wide variety of conceptual designs for hypersonic airbreathing vehicles. With the tools provided herein, an important parameter, such as the inlet contraction ratio, can be systematically varied to examine its effect on the vehicle design and performance to identify optimal configurations. Moreover, many of the resulting geometric features

of these designs, such as swept leading edges, lead to concomitant benefits.

References

[1]Billig, F. S., "Supersonic Combustion Ramjet Missile," *Journal of Propulsion and Power*, Vol. 11, No. 6, 1995, pp. 1139–1146.

[2]Molder, S., and Szpiro, E. J., "Busemann Inlet for Hypersonic Speeds," *Journal of Spacecraft and Rockets*, Vol. 3, No. 8, 1966, pp. 1172–1176.

[3]Kothari, A. P., Tarpley, C., McLaughlin, T. A., Suresh, B., and Livingston, J. W., "Hypersonic Vehicle Design Using Inward Turning Flowfields," AIAA Paper 96-2552, July 1996.

[4]Billig, F. S., Corda, S., and Stockbridge, R. D., "Combustor Inlet Interactions in Scramjet Engines," *APL Technical Review*, Vol. 2, No. 1, 1990, pp. 359–383.

[5]Agosta, V. D., and Hammer, S. S., "Scramjet Nozzle Analysis," Propulsion Sciences, Inc., PSI Rept. 70-1, Melville, NY, Feb. 1970.

[6]Agosta, V. D., Hammer, S., and Migdal, D., "Scramjet Nozzle Analysis," Propulsion Sciences, Inc., Final Rept. to Johns Hopkins Univ. Applied Physics Lab., Melville, NY, Feb. 1971.

[7]Billig, F. S., Funk, J. A., Lasky, M., and Dugger, G. L., "SCRAM Free Jet Testing, Component Design and Performance," *1971 JANNAF Combined Propulsion Meeting CPIA Publication 219*, Johns Hopkins Univ. Applied Physics Lab., Laurel, MD, Vol. 3, 1971, pp. 359–383.

[8]Lucero, E. F., "SCRAM Aerodynamic Design," Johns Hopkins Univ. Applied Physics Lab., C-RQR/73-4, Research and Development Programs Quarterly Rept., 1973.